Frequency-Domain Design of Asymmetric Circular Differential Microphone Arrays

Yaakov Buchris, *Member, IEEE*, Israel Cohen, *Fellow, IEEE*, and Jacob Benesty

***Abstract*—Circular differential microphone arrays (CDMAs) facilitate compact superdirective beamformers whose beampatterns are nearly frequency invariant. In contrast to linear differential microphone arrays where the optimal steering direction is at the endfire, CDMAs provide perfect steering for all azimuthal directions. Herein, we extend the traditional symmetric model of DMAs and establish an analytical asymmetric model for Nth-order CDMAs. This model exploits the circular geometry to eliminate the inherent limitation of symmetric beampatterns associated with a linear geometry and allows also asymmetric beampatterns. This new model is then used to develop asymmetric versions of two optimal commonly used beampatterns namely the hypercardioid and the supercardioid. Experimental results demonstrate the advantages of the asymmetric model compared to the traditional symmetric one, when additional directional constraints are imposed. The proposed model yields superior performance in terms of white noise gain, directivity factor, and front-to-back ratio, as well as more flexible design of nulls for the interfering signals.**

***Index Terms*—Circular differential microphone arrays, asymmetric beampatterns, broadband beamforming, hypercardioid, supercardioid.**

I. Introduction

DIFFERENTIAL microphone arrays (DMAs) refer to arrays that combine closely spaced sensors to respond to the spatial derivatives of the acoustic pressure field. These small-size arrays yield nearly frequency-invariant beampatterns. Moreover, DMAs include the well-known superdirective beamformer [1], [2] as a particular case. Therefore, DMAs have attracted much research interest in recent years.

DMAs first appeared in the literature in the 1930's, designed to respond to the spatial derivatives of an acoustic pressure field [3], and later were implemented using omnidirectional pressure microphones [4]. These early fixed implementations had a prominent limitation that once they were designed and produced, their properties cannot be changed. The modern concept of DMAs employs pressure microphones, and digital signal processing techniques are used to obtain desired directional responses [5]–[9]. Based on the modern concept, several works on DMAs appeared during the last two decades. Buck [10], and Derkx and Janse [11] analyzed the performance of the first-order design under array imperfections, and presented solutions for sensors calibration. First- and second- order adaptive DMAs based on fullband as well as on subband algorithms were introduced and examined by Teutsch and Elko [12]. De Sena *et al.* [13] proposed a general approach to the design of directivity patterns of higher-order DMAs. In [14] a more general approach is proposed for the design of DMAs, which ignores the traditional differential structure of DMAs and develops broadband frequency-domain DMAs up to any order from a signal processing perspective. Robust frequency-domain DMAs have been presented by Zhao *et al.* [15], and Pan *et al.* [16]. More recent work on DMAs can be found in [17]–[20].

Most of the work on DMAs deals with a linear array geometry. The geometry of microphone arrays plays an important role in the formulation, solution, and performance of the algorithms. The selection of the geometry, however, depends heavily on the application requirements. For example, in devices like smartphones, tablet PCs, and smart televisions, a linear geometry is preferable as this type of arrays can be easily integrated into the devices. But linear arrays may not have the same response at different directions as shown in [21]. In applications like teleconferencing and 3D sound recording where the signal of interest may come from any direction, it is necessary for the microphone array to have similar, if not the same response from one direction to another. In such cases, circular arrays are advantageous.

Design schemes of circular arrays can be classified into two main categories. The first category relies on narrow-band methods for the design of frequency-varying beampatterns [22]–[28]. The second category incorporates methods that produce frequency-invariant beampatterns [29]–[32]. A general approach for the design of frequency-invariant broadband beamformers is to solve an optimization problem which enforces several constraints in the frequency domain, such as frequency-invariant beampattern either in all angular directions or only in specific directions like the mainbeam direction. Other constraints may be imposed to ensure an adequate performance level such as maximum white noise gain WNG.

Recently, Benesty *et al.* [33] presented a study of the most basic concepts and fundamental techniques used in the design

Manuscript received February 13, 2017; revised August 13, 2017 and December 31, 2017; accepted January 8, 2018. Date of publication January 23, 2018; date of current version February 8, 2018. This work was supported in part by the Israel Science Foundation under Grant 576/16, in part by the ISF-NSFC joint research program under Grant 2514/17, and in part by the MAFAAT-Israel Ministry of Defense. The associate editor coordinating the review of this manuscript and approving it for publication was Dr. Alexey Ozerov. *(Corresponding author: Yaakov Buchris.)*

Y. Buchris and I. Cohen are with the Department of Electrical Engineering, Technion—Israel Institute of Technology, Haifa 3200003, Israel (e-mail: sbucris@gmail.com; icohen@ee.technion.ac.il).

J. Benesty is with the Universite du Quebec INRS-EMT, Montreal, QC G1K 9H7, Canada (e-mail: benesty@emt.inrs.ca).

Color versions of one or more of the figures in this paper are available online at http://ieeexplore.ieee.org.

Digital Object Identifier 10.1109/TASLP.2018.2796844

and implementation of different orders of circular differential microphone arrays (CDMAs). In [34], we introduced a time-domain design for first-order CDMAs.

Existing works on DMAs, for linear or circular geometry, consider only the case of symmetric beampatterns, which is an inherent property of the linear geometry and confines the design process by some aspects. For linear arrays, a symmetric beampattern means that the beampattern is symmetric with respect to the axis of the array. Such a symmetry is not required in different array geometries like the circular geometry, thus, removing this requirement may lead to a substantial performance improvement. We term such beampatterns as asymmetric beampatterns.

In this paper, we derive an analytical model for asymmetric CDMAs which includes also the traditional symmetric model as a particular case. We begin with an extension of the well-known analytical expression for the directivity pattern of the traditional DMAs, to a generalized expression which supports also the asymmetric case. Next, we derive asymmetric versions for two popular directivity patterns usually applied in the context of microphone arrays, namely the hypercardioid and the supercardioid which are designed to maximize the directivity factor (DF) and the front-to-back ratio (FBR), respectively [6]. Originally, both directivity patterns were developed for the symmetric framework as unconstrained versions, i.e., no directional constraints were imposed except the distortionless constraint in the desired source direction. Herein, we derive constrained versions where additional directional attenuation constraints are imposed. For that case, the asymmetric design achieves better performance with respect to the traditional one, since it enables more flexible design. As expected, the solutions for the asymmetric design are reduced to the solutions presented in [6] where no additional directional attenuation constraints are imposed.

We should note that an asymmetric design of CDMAs was already presented in [33, ch.6] but only for the case of a superdirective beamformer with a single distortionless constraint in the desired source direction. Herein, we present a more general framework for asymmetric design of CDMAs, which is based on the analytical proposed model of the asymmetric beampattern, and enables to derive analytical expressions for both the asymmetric hypercardioid and the supercardioid directivity patterns as well as other general directivity patterns. Yet, for the particular case of optimizing the DF under the distortionless constraint, both solutions are consolidated.

The frequency-invariant beampattern produced by the proposed analytical asymmetric model is then used as the input desired beampattern for a general practical design of Nth-order CDMAs, which enables perfect steering to any azimuthal direction. We show that the solution design proposed in [33], which is based on symmetry, is a particular case of the proposed practical design. In the simulations section, we demonstrate the main advantages of the asymmetric model and compare it to the symmetric one. It is shown that the asymmetric model achieves better performance in terms of WNG, DF, and FBR due to a more flexible design, which takes into account the requirements regarding the null directions. Furthermore, additional degrees of freedom are available for a given number of null directions which can be utilized to choose CDMAs of reduced orders with respect to the minimal order in the symmetric model, and improve robustness to array imperfections.

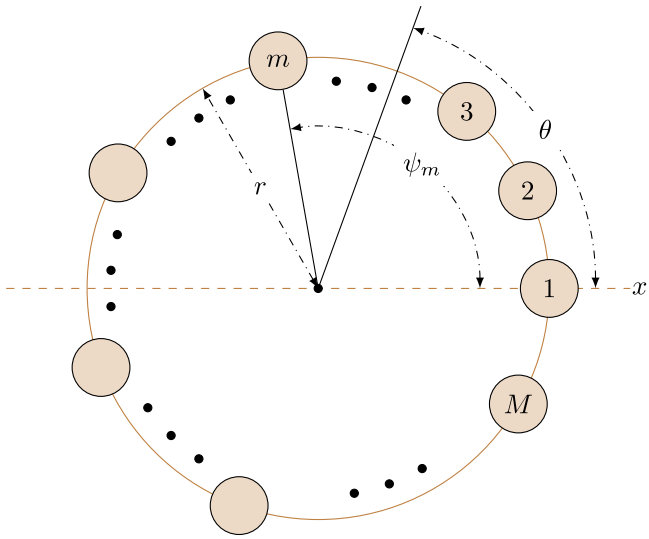

Fig. 1. Illustration of a uniform circular microphone array in the Cartesian coordinate system.

The paper is organized as follows. In Section II, we formulate the signal model. In Section III, we concisely present the traditional symmetric model of Nth-order CDMAs. In Section IV, we derive asymmetric beampatterns for CDMAs and also develop the equivalent asymmetric hypercardioid and supercardioid. In Section V, we present an Nth-order CDMA practical design for a given number of sensors. Section VI demonstrates some design examples.

II. Signal Model

We consider an acoustic source signal, $X(\omega)$, with ω being the angular frequency, that propagates in an anechoic acoustic environment at the speed of sound, i.e., $c \approx 340$ m/s, and impinges on a uniform circular array (UCA) of radius r, consisting of M omnidirectional microphones, where the distance between two successive sensors is equal to

$$\delta = 2r \sin\left(\frac{\pi}{M}\right) \approx \frac{2\pi r}{M}. \tag{1}$$

The direction of the source signal to the array is denoted by the azimuth angle θ_{s}. We assume that the center of the UCA coincides with the origin of the Cartesian coordinate system and serves also as the reference. Azimuth angles are measured anti-clockwise from the x axis, i.e., at $\theta = 0^\circ$, and sensor 1 of the array is placed on the x axis, i.e., at $\theta = 0^\circ$, as illustrated in Fig. 1.

Assuming the far-field propagation, the time delay between the mth microphone and the center of the array is

$$t_m(\theta_{\mathrm{s}}) = \frac{r}{c}\cos\left(\theta_{\mathrm{s}} - \psi_m\right),\ m = 1, 2, \ldots, M, \tag{2}$$

where

$$\psi_m = \frac{2\pi(m-1)}{M} \tag{3}$$

is the angular position of the mth array element. The mth microphone signal is given by

$$Y_m(\omega) = e^{j\varpi\cos(\theta_s-\psi_m)}X(\omega) + V_m(\omega),\ m = 1,\ldots,M, \tag{4}$$

where $\varpi = \frac{\omega r}{c}$, $j = \sqrt{-1}$ is the imaginary unit, and $V_m(\omega)$ is the additive noise at the mth microphone. In a vector form, (4) becomes

$$\begin{aligned}\mathbf{y}(\omega) =&\ [Y_1(\omega)\ Y_2(\omega)\ \cdots\ Y_M(\omega)]^T\\ =&\ \mathbf{d}(\omega,\theta_s)X(\omega) + \mathbf{v}(\omega),\end{aligned} \tag{5}$$

where the superscript ^{T} denotes the transpose operator, $\mathbf{d}(\omega,\theta_s)$ is the steering vector at $\theta = \theta_s$, i.e.,

$$\begin{aligned}\mathbf{d}(\omega,\theta_s) =&\ \left[e^{j\omega t_1(\theta_s)}\cdots e^{j\omega t_M(\theta_s)}\right]^T\\ =&\ \left[e^{j\varpi\cos(\theta_s-\psi_1)}\cdots e^{j\varpi\cos(\theta_s-\psi_M)}\right]^T,\end{aligned} \tag{6}$$

the vector $\mathbf{v}(\omega)$ is defined similarly to $\mathbf{y}(\omega)$, and the acoustic wavelength is $\lambda = c/f$. According to the model of the DMAs, it is assumed that the element spacing, δ, is much smaller than the wavelength of the incoming signal, i.e.,

$$\delta \ll \lambda, \tag{7}$$

or, equivalently,

$$\varpi \ll M, \tag{8}$$

in order to approximate the differential of the pressure signal.

III. Traditional Symmetric Nth-Order CDMAs

Traditional Nth-order CDMAs were designed to have a symmetric directivity pattern. The directivity pattern describes the sensitivity of the beamformer to a plane wave impinging on the UCA from the direction specified by the pair (θ,ϕ) where θ is the azimuth and ϕ is the elevation. In this paper, we confine ourselves to the 2D case of $\phi = \pi/2$, i.e., the plane where the UCA is laid. The 3D case is a subject to a future research. For the 2D case, the frequency-invariant beampattern of an Nth-order DMA is given, for any steering angle θ_s, as [6]

$$\mathcal{B}_N(\theta-\theta_s) = \sum_{n=0}^{N} a_{N,n}\cos^n(\theta-\theta_s), \tag{9}$$

where $\{a_{N,n}\}_{n=0}^{N}$ are real coefficients. The beampattern $\mathcal{B}_N(\theta-\theta_s)$ is an even function as it is a power series of the cosine function.

Modern Nth-order DMAs have a time-domain hierarchical delay-and-subtract structure and originally proposed for the linear geometry [6]. In general, the response of an Nth-order DMA is proportional to a linear combination of signals derived from spatial derivatives from order 0 to (including) order N and corresponds to the Nth level in the hierarchical structure.

Traditional designs of DMAs focused mainly on the linear geometry which inherently dictates a symmetric beampattern, thus (9) was sufficient for the description of frequency-invariant beampatterns associated with DMAs. Herein, we introduce an asymmetric model for the directivity pattern of Nth-order CDMAs, which exploits the circular structure and incorporates both symmetric and asymmetric beampatterns.

IV. Asymmetric Beampattern for CDMAs

In this section, we extend the traditional analytical symmetric beampattern (9) and derive an asymmetric beampattern for CDMAs, where asymmetry means that the beampattern is not confined to be symmetric with respect to the steering angle θ_s, i.e., in the general case $\mathcal{B}_N(\theta-\theta_s) \neq \mathcal{B}_N(-\theta+\theta_s)$. Later, we will see that such a generalized model leads to a more flexible design of CDMAs.

A. Asymmetric Beampattern of Nth-Order CDMAs

We start with the simple first-order asymmetric case and then we generalize it for any desired order, N. First-order CDMAs can be designed with at least three microphones (the case of only two microphones is consolidated with the linear case which was extensively investigated in [14]). The geometry of first-order CDMAs is an equilateral triangle of radius r and the sensor spacing is $\delta = 2r\sin(\pi/3) = \sqrt{3}r$. The positions of the three microphones are

$$\psi_1 = 0, \psi_2 = \frac{2\pi}{3}, \psi_3 = \frac{4\pi}{3}. \tag{10}$$

Assuming a 2D propagation model (i.e., $\phi = \pi/2$), the acoustic propagation field received at each sensor can be expressed as

$$p(k,r,\theta,\psi_m) = P_0 e^{-j\varpi\cos(\theta-\psi_m)},\ m = 1,2,3, \tag{11}$$

where P_0 is the plane-wave amplitude, and $k = \frac{\omega}{c}$ is the wave number. We may add a complex gain $c_m e^{-j\omega\tau_m}$ at each sensor, sum all the sensors' outputs, and get the output pressure:

$$p_o(k,r,\theta) = P_0\sum_{m=1}^{3} c_m e^{-j\omega\tau_m} e^{-j\varpi\cos(\theta-\psi_m)}, \tag{12}$$

where c_m is a real number, and τ_m is a temporal delay added to the signal acquired by the mth microphone. Without loss of generality, we assume that $P_0 = 1$, $c_1 = 1$, and $\tau_1 = 0$. Using the approximation that $e^{-x} \approx 1 - x$, (12) becomes

$$\begin{aligned}p_o(k,r,\theta) \approx&\ 1 + c_2 + c_3\\ &- j\omega\sum_{m=1}^{3} c_m\left[\tau_m + \frac{r}{c}\cos(\theta-\psi_m)\right],\end{aligned} \tag{13}$$

where this approximation holds for small values of $\omega\tau_m$ and ϖ in accordance with the DMAs' model Assumptions (7) and (8). In order to cancel DC components which have no influence on the shape of the directional response of the array, we impose

$c_1 + c_2 + c_3 = 0$, leading to $c_2 + c_3 = -1$, and define

$$\alpha_1 = \frac{\sum_{m=1}^{3} c_m \tau_m}{\sum_{m=1}^{3} c_m \left(\tau_m + \frac{r}{c}\cos\psi_m\right)}, \tag{14}$$

$$1 - \alpha_1 = \frac{\sum_{m=1}^{3} c_m \frac{r}{c}\cos\psi_m}{\sum_{m=1}^{3} c_m \left(\tau_m + \frac{r}{c}\cos\psi_m\right)}, \tag{15}$$

$$\beta_1 = \frac{\sum_{m=1}^{3} c_m \frac{r}{c}\sin\psi_m}{\sum_{m=1}^{3} c_m \left(\tau_m + \frac{r}{c}\cos\psi_m\right)}. \tag{16}$$

Now we can write the normalized response of the first-order asymmetric CDMA as

$$\mathcal{B}_1(\theta) = \frac{p_{\mathrm{o}}(k,r,\theta)}{p_{\mathrm{o}}(k,r,0)} = \alpha_1 + (1-\alpha_1)\cos\theta + \beta_1 \sin\theta. \tag{17}$$

It can be easily noticed that the last expression is a generalization of the well-known first-order DMA response [6]. Thus, the proposed design includes also the symmetric design as a particular case. It should be noted that although the normalized response is frequency-invariant, the output pressure (13) includes also a first-order high-pass frequency response, which can be compensated by a first-order low-pass filter [5], [6]. We later see in Section V that by implementing asymmetric CDMAs using a more general design approach in the frequency domain, this high-pass response is inherently compensated.

Note that since we imposed $c_2 + c_3 = -1$, (12) can be rewritten as

$$\begin{aligned} p_{\mathrm{o}}(k,r,\theta) &= x\left[e^{-j\varpi\cos(\theta-\psi_1)} - e^{-j\omega\tau_2 - j\varpi\cos(\theta-\psi_2)}\right] \\ &\quad + (1-x)\left[e^{-j\varpi\cos(\theta-\psi_1)}\right. \\ &\quad \left. - e^{-j\omega\tau_3 - j\varpi\cos(\theta-\psi_3)}\right], \end{aligned} \tag{18}$$

where $x = -c_2$. Therefore, (18) can be interpreted as a weighted sum of the differential of the pressure measured between sensor 1 and sensor 2 and the differential of the pressure measured between sensor 1 and sensor 3. In other words, the first-order output of CDMAs is a linear combination of two first-order linear DMAs outputs.

The fact that DMAs have a hierarchical multistage structure [6] implies that the response of Nth-order DMAs can be described as a cascade of first-order responses, i.e., the total response of Nth-order CDMAs is a product of N responses of first-order DMAs. For example, every two outputs of first-order DMAs on the first stage are the inputs to another first-order DMA in the next stage. When a beamformer is implemented in a multistage way, its beampattern equals the product of the beampatterns of all the different stages [18]. Therefore, the second-order asymmetric CDMA's beampattern can be written as a product of two first-order terms, i.e.,

$$\mathcal{B}_2(\theta) = \prod_{i=1}^{2}\left[\alpha_i + (1-\alpha_i)\cos\theta + \beta_i \sin\theta\right], \tag{19}$$

from which we can easily derive the general form of the second-order asymmetric CDMA:

$$\mathcal{B}_2(\theta) = \upsilon_0 + \upsilon_1\cos\theta + \upsilon_2\cos^2\theta + \upsilon_3\sin\theta\cos\theta + \upsilon_4\sin\theta, \tag{20}$$

where $\{\upsilon_i\}_{i=0}^{4}$ are real coefficients which depend on $\{\alpha_i, \beta_i\}_{i=1}^{2}$. Repeating on similar steps, the following general expressions for the third and fourth orders can be derived, respectively,

$$\begin{aligned} \mathcal{B}_3(\theta) &= \epsilon_0 + \epsilon_1\cos\theta + \epsilon_2\cos^2\theta + \epsilon_3\cos^3\theta \\ &\quad + \epsilon_4\sin\theta\cos\theta + \epsilon_5\sin\theta + \epsilon_6\sin^3\theta \end{aligned} \tag{21}$$

and

$$\begin{aligned} \mathcal{B}_4(\theta) &= \eta_0 + \eta_1\cos\theta + \eta_2\cos^2\theta + \eta_3\cos^3\theta + \eta_4\cos^4\theta \\ &\quad + \eta_5\sin\theta\cos\theta + \eta_6\sin^3\theta\cos\theta \\ &\quad + \eta_7\sin\theta + \eta_8\sin^3\theta. \end{aligned} \tag{22}$$

Based on the last results, we can obtain the Nth-order asymmetric CDMA beampattern with the mainlobe steered to θ_{s}:

$$\begin{aligned} \mathcal{B}_N(\theta-\theta_{\mathrm{s}}) &= \sum_{n=0}^{N}\xi_n\cos^n(\theta-\theta_{\mathrm{s}}) \\ &\quad + \sum_{n=0}^{\lfloor\frac{N-1}{2}\rfloor}\mu_n\sin^{2n+1}(\theta-\theta_{\mathrm{s}}) \\ &\quad + \sum_{n=1}^{\lfloor\frac{N}{2}\rfloor}\zeta_n\cos(\theta-\theta_{\mathrm{s}})\sin^{2n-1}(\theta-\theta_{\mathrm{s}}), \end{aligned} \tag{23}$$

which is a trigonometric polynomial of power N with $2N$ roots. Note that (23) is a general expression for the beampattern which can be reduced to the traditional symmetric beampattern (9) by setting the coefficients $\{\zeta_n, \mu_n\}_n$ to zero.

In order to prove that (23) is indeed the general theoretical expression for all possible beampatterns of CDMAs of order N, we may refer to the Fourier theorem stating that each function $f(\theta) \in \mathbb{F}$, where $\mathbb{F}$ is the space of continuous functions in $[-\pi, \pi]$, can be represented by the infinite series:

$$f(\theta) = \sum_{n=0}^{\infty}\left[a_n\cos(n\theta) + b_n\sin(n\theta)\right], \tag{24}$$

where

$$a_n = \frac{1}{\pi}\int_{-\pi}^{\pi} f(\theta)\cos(n\theta)\,d\theta,\ \ n = 0,1,2,\ldots \tag{25}$$

$$b_n = \frac{1}{\pi}\int_{-\pi}^{\pi} f(\theta)\sin(n\theta)\,d\theta,\ \ n = 0,1,2,\ldots \tag{26}$$

Let $f_N(\theta) \in \mathbb{F}_N \subset \mathbb{F}$, where $\mathbb{F}_N$ is a subspace of all the continuous functions in $[-\pi, \pi]$, which can be represented by the following finite series:

$$f_N(\theta) = \sum_{n=0}^{N}\left[a_n\cos(n\theta) + b_n\sin(n\theta)\right]. \tag{27}$$

In the Appendix, we show that every function $f_N(\theta) \in \mathbb{F}_N$ can also be represented by (23). Actually, we show that the space of functions specified by (27) is equivalent to the space of functions specified by (23) for each N. This equivalence ensures that for an Nth-order beampattern, only the basis functions $\{\cos(n\theta), \sin(n\theta)\}_{n=0}^{N}$ are required. Since it is true for each N and particularly when $N \to \infty$, it is obvious that (23) is the general expression for any Nth-order asymmetric beampattern. Therefore, we can express (23) more compactly as

$$\mathcal{B}_N(\theta - \theta_s) = \sum_{n=0}^{N} a_n \cos[n(\theta - \theta_s)] + \sum_{n=1}^{N} b_n \sin[n(\theta - \theta_s)]. \tag{28}$$

Note that (28) is a trigonometric polynomial with $2N+1$ coefficients, which implies that at least $2N+1$ sensors are required in order to implement Nth-order asymmetric CDMAs, as will be discussed in Section V. In contrast, the traditional symmetric beampattern (9) is a trigonometric polynomial with $N+1$ coefficients, which implies that only $N+1$ sensors are required for implementing symmetric Nth-order DMAs. While this is true for the linear geometry, for the circular geometry, still at least $2N$ sensors are required as presented in [33].

In the next subsections, we develop the equivalent hypercardioid and the equivalent supercardioid optimal patterns for the case of asymmetric CDMAs. For convenience, we use (28) instead of (23).

B. Optimal Asymmetric Hypercardioid

The most common directivity patterns in the context of microphone arrays are the dipole, cardioid, hypercardioid, and supercardioid, which were obtained via optimization with respect to various criteria. For example, the hypercardioid was designed to maximize the DF of the array which is the gain in signal-to-noise ratio (SNR) for the case of diffuse noise. These patterns, originally developed for the linear geometry, are traditionally symmetric with respect to the steering angle, θ_s.

The proposed analytical model for the asymmetric beampattern of CDMAs (28) can be used to produce several beampatterns which can be controlled by the adjustment of its coefficients. In this section, we derive the equivalent asymmetric hypercardioid, i.e., the beampattern that maximizes the DF, which is defined as (see for example [35, ch.2])

$$\mathcal{D} = \frac{\mathcal{B}^2(\theta_s, \phi_s)}{\frac{1}{4\pi}\int_0^{2\pi}\int_0^{\pi} \mathcal{B}^2(\theta, \phi)\sin\phi d\phi d\theta}, \tag{29}$$

where $\mathcal{B}(\theta, \phi)$ is a 3D beampattern and (θ_s, ϕ_s) specifies the steering direction. In our study, we are concentrating on the 2D scenario for which the beampattern is a function of only the azimuthal angle, θ, i.e.,

$$\mathcal{B}_N(\theta - \theta_s) = \mathcal{B}(\theta - \theta_s, \phi = \pi/2), \tag{30}$$

and (29) is actually the DF for the cylindrical noise field model. A cylindrical noise field model is often assumed for scenarios where the reflections from the floor or the ceiling of the room are negligible. Without loss of generality, we assume that $\theta_s = 0^\circ$. It is obvious that

$$\mathcal{D}^{-1} = \frac{1}{2\pi}\int_0^{2\pi} \mathcal{B}_N^2(\theta)\, d\theta. \tag{31}$$

From Fourier Theorem it is known that the basis functions $\{\cos(n\theta), \sin(n\theta)\}_{n=0}^{\infty}$ that appear in (28) form a complete orthonormal system, therefore it is straightforward to show that

$$\int_0^{2\pi} \mathcal{B}_N^2(\theta)\, d\theta = \mathbf{c}^T \mathbf{\Gamma}_{\mathrm{h}} \mathbf{c}, \tag{32}$$

where

$$\mathbf{c} = [a_0, a_1, \ldots, a_N, b_1, \ldots, b_N]^T \tag{33}$$

is a vector of length $2N+1$ containing the coefficients of the asymmetric beampattern (28), and the matrix $\mathbf{\Gamma}_{\mathrm{h}}$ is diagonal of size $(2N+1)\times(2N+1)$, where its diagonal elements are

$$[\mathbf{\Gamma}_{\mathrm{h}}]_{n,n} = \begin{cases} \int_0^{2\pi} \cos^2(n\theta)\, d\theta, & n = 0, 1, \ldots, N \\ \int_0^{2\pi} \sin^2[(n-N)\theta]\, d\theta, & n = N+1, \ldots, 2N. \end{cases} \tag{34}$$

Calculation of (34) yields the following compact expression:

$$\mathbf{\Gamma}_{\mathrm{h}} = \pi \mathrm{diag}\left(\left[2, \mathbf{1}_{2N}^T\right]^T\right), \tag{35}$$

where $\mathrm{diag}(\mathbf{x})$ is a diagonal matrix with the elements of the vector $\mathbf{x}$ on its diagonal, and $\mathbf{1}_{2N}$ is a $2N \times 1$ column vector with all elements equal to one.

According to (31), maximizing the DF is equivalent to minimizing (32). Yet, minimizing (32) without any constraints will obviously lead to the trivial solution $\mathbf{c} = \mathbf{0}$. Therefore, at least one directional constraint should be imposed, either for the symmetric design or the asymmetric design, namely the distortionless constraint:

$$\mathcal{B}_N(\theta_s = 0^\circ) = 1, \tag{36}$$

which leads to

$$\sum_{n=0}^{N} a_n = 1. \tag{37}$$

One can see that (37) constrains the coefficients $\{a_n\}_{n=0}^{N}$ to each other, but still the coefficients $\{a_n\}_{n=0}^{N}$ and $\{b_n\}_{n=1}^{N}$ are independent by the diagonality of $\mathbf{\Gamma}_{\mathrm{h}}$. Thus, the circular geometry provides additional degrees of freedom in the design of optimal patterns such as the hypercardioid, which can be exploited to achieve higher performance when it is desirable to impose additional directional constraints. In that case, we can add up to $L \leq 2N$ attenuation constraints of the form:

$$\mathcal{B}_N(\theta = \theta_l) = g_l,\ l = 1, 2, \ldots, L, \tag{38}$$

where $0 \leq g_l \leq 1$. We formulate these constraints as

$$\mathbf{H}_{\mathrm{c}} \mathbf{c} = \mathbf{g}, \tag{39}$$

where $\mathbf{H}_{\mathrm{c}}$ is the constraint matrix of size $(L+1)\times(2N+1)$. The vector $\mathbf{g}$ of length $L+1$ contains the coefficients g_l, $l = 1, 2, \ldots, L$, and a single unity entry satisfying (36).

The optimization problem for the asymmetric hypercardioid beampattern can be formulated as

$$\min_{\mathbf{c}} \ \mathbf{c}^T\mathbf{\Gamma}_{\mathrm{h}}\mathbf{c} \ \ \text{subject to} \ \ \mathbf{H}_{\mathrm{c}}\mathbf{c}=\mathbf{g}. \tag{40}$$

Using the method of Lagrange multipliers, we get the following closed-form expression:

$$\mathbf{c}_{\mathrm{opt}}=\mathbf{\Gamma}_{\mathrm{h}}^{-1}\mathbf{H}_{\mathrm{c}}^T\left[\mathbf{H}_{\mathrm{c}}\mathbf{\Gamma}_{\mathrm{h}}^{-1}\mathbf{H}_{\mathrm{c}}^T\right]^{-1}\mathbf{g}. \tag{41}$$

This solution yields the optimal asymmetric hypercardioid CDMA for a cylindrical noise field. Note that even though we can add up to $2N$ constraints, it is obvious that a lower number of attenuation constraints leads to a more flexibility and higher DF. Specifically, if we add exactly $2N$ attenuation constraints, (40) has no meaning and (39) should be solved directly. Moreover, if no additional constraints except (36) are imposed, (41) reduces to the solution of the symmetric unconstrained hypercardioid in [6]. In Section VI-A, two design examples of a second-order asymmetric hypercardioid are presented and compared to the symmetric design.

C. Optimal Asymmetric Supercardioid

In this section, we develop the asymmetric version of the supercardioid for CDMAs. The supercardioid pattern maximizes the FBR of an array [6], which is defined as the ratio between the directional gain of the microphone to signals propagating to the front of the microphone relative to signals propagating to the rear. For a cylindrical noise field, the FBR is defined as

$$\mathcal{F}=\frac{\int_{-\pi/2}^{\pi/2}\mathcal{B}_N^2\left(\theta\right)d\theta}{\int_{\pi/2}^{3\pi/2}\mathcal{B}_N^2\left(\theta\right)d\theta}, \tag{42}$$

where we assume, without loss of generality, that the steering angle is $\theta_{\mathrm{s}}=0^\circ$. Similarly to the hypercardioid, it can be shown that

$$\int_{-\pi/2}^{\pi/2}\mathcal{B}_N^2\left(\theta\right)d\theta=\mathbf{c}^T\mathbf{\Gamma}_{\mathrm{f}}\mathbf{c} \tag{43}$$

and

$$\int_{\pi/2}^{3\pi/2}\mathcal{B}_N^2\left(\theta\right)d\theta=\mathbf{c}^T\mathbf{\Gamma}_{\mathrm{b}}\mathbf{c}, \tag{44}$$

where the vector $\mathbf{c}$ is defined in (33), and the matrices $\mathbf{\Gamma}_{\mathrm{f}}$ and $\mathbf{\Gamma}_{\mathrm{b}}$ are diagonal, with

$$\left[\mathbf{\Gamma}_{\mathrm{f}}\right]_{n,n}=\begin{cases}\int_{-\pi/2}^{\pi/2}\cos^2\left(n\theta\right)d\theta, & n=0,1,\ldots,N\\ \int_{-\pi/2}^{\pi/2}\sin^2\left[(n-N)\theta\right]d\theta, & n=N+1,\ldots,2N\end{cases} \tag{45}$$

and

$$\left[\mathbf{\Gamma}_{\mathrm{b}}\right]_{n,n}=\begin{cases}\int_{\pi/2}^{3\pi/2}\cos^2\left(n\theta\right)d\theta, & n=0,1,\ldots,N\\ \int_{\pi/2}^{3\pi/2}\sin^2\left[(n-N)\theta\right]d\theta, & n=N+1,\ldots,2N.\end{cases} \tag{46}$$

Similarly to $\mathbf{\Gamma}_{\mathrm{h}}$, both $\mathbf{\Gamma}_{\mathrm{f}}$ and $\mathbf{\Gamma}_{\mathrm{b}}$ can be expressed in a compact form as

$$\mathbf{\Gamma}_{\mathrm{f}}=\mathbf{\Gamma}_{\mathrm{b}}=\frac{\pi}{2}\mathrm{diag}\left(\left[2,\mathbf{1}_{2N}^T\right]^T\right). \tag{47}$$

Like in the previous case of the hypercardioid, we can add the linear directional constraints specified by (39) in order to achieve some benefits from the asymmetric framework. Now we can formulate the optimization problem which provides the asymmetric supercardioid beampattern:

$$\max_{\mathbf{c}} \ \frac{\mathbf{c}^T\mathbf{\Gamma}_{\mathrm{f}}\mathbf{c}}{\mathbf{c}^T\mathbf{\Gamma}_{\mathrm{b}}\mathbf{c}} \ \ \text{subject to} \ \mathbf{H}_{\mathrm{c}}\mathbf{c}=\mathbf{g}. \tag{48}$$

Rather than solving (48), we solve the equivalent problem:

$$\max_{\hat{\mathbf{c}}} \frac{\hat{\mathbf{c}}^T\hat{\mathbf{\Gamma}}_{\mathrm{f}}\hat{\mathbf{c}}}{\hat{\mathbf{c}}^T\hat{\mathbf{\Gamma}}_{\mathrm{b}}\hat{\mathbf{c}}} \ \ \text{subject to} \ \hat{\mathbf{H}}_{\mathrm{c}}\hat{\mathbf{c}}=\mathbf{0}, \tag{49}$$

where

$$\hat{\mathbf{c}}=\begin{bmatrix}\mathbf{c}\\ -1\end{bmatrix},\ \hat{\mathbf{H}}_{\mathrm{c}}=\begin{bmatrix}\mathbf{H}_{\mathrm{c}} & \mathbf{g}\end{bmatrix},\ \hat{\mathbf{\Gamma}}_{\mathrm{f}}=\begin{bmatrix}\mathbf{\Gamma}_{\mathrm{f}} & \mathbf{0}\\ \mathbf{0}^T & 0\end{bmatrix},$$
$$\hat{\mathbf{\Gamma}}_{\mathrm{b}}=\begin{bmatrix}\mathbf{\Gamma}_{\mathrm{b}} & \mathbf{0}\\ \mathbf{0}^T & 0\end{bmatrix}. \tag{50}$$

Let $\mathbf{D}$ be a null-space matrix of $\hat{\mathbf{H}}_{\mathrm{c}}$ (i.e., $\hat{\mathbf{H}}_{\mathrm{c}}\mathbf{D}=\mathbf{0}$) of size $(2N+2)\times(2N+1-L)$ and rank of $2N+1-L$, which contains $2N+1-L$ basis vectors in its columns, and let $\hat{\mathbf{c}}=\mathbf{D}\tilde{\mathbf{c}}$. Note that the matrices $\mathbf{D}^T\hat{\mathbf{\Gamma}}_{\mathrm{f}}\mathbf{D}$ and $\mathbf{D}^T\hat{\mathbf{\Gamma}}_{\mathrm{b}}\mathbf{D}$ are full-rank even though $\hat{\mathbf{\Gamma}}_{\mathrm{f}}$ and $\hat{\mathbf{\Gamma}}_{\mathrm{b}}$ are not full rank since the product matrices $\mathbf{D}^T\hat{\mathbf{\Gamma}}_{\mathrm{f}}\mathbf{D}$ and $\mathbf{D}^T\hat{\mathbf{\Gamma}}_{\mathrm{b}}\mathbf{D}$ are of size $(2N+1-L)\times(2N+1-L)$ with a rank of $(2N+1-L)$, i.e, full-rank matrices. Thus, we transform (49) to the following unconstrained optimization problem [36], [37]:

$$\max_{\tilde{\mathbf{c}}} \frac{\tilde{\mathbf{c}}^T\mathbf{D}^T\hat{\mathbf{\Gamma}}_{\mathrm{f}}\mathbf{D}\tilde{\mathbf{c}}}{\tilde{\mathbf{c}}^T\mathbf{D}^T\hat{\mathbf{\Gamma}}_{\mathrm{b}}\mathbf{D}\tilde{\mathbf{c}}}. \tag{51}$$

The solution to (51) is the generalized eigenvector of $\mathbf{D}^T\hat{\mathbf{\Gamma}}_{\mathrm{f}}\mathbf{D}$ and $\mathbf{D}^T\hat{\mathbf{\Gamma}}_{\mathrm{b}}\mathbf{D}$ that corresponds to the maximal generalized eigenvalue, i.e.,

$$\mathbf{D}^T\hat{\mathbf{\Gamma}}_{\mathrm{f}}\mathbf{D}\tilde{\mathbf{c}}_{\mathrm{opt}}=\lambda_{\max}\mathbf{D}^T\hat{\mathbf{\Gamma}}_{\mathrm{b}}\mathbf{D}\tilde{\mathbf{c}}_{\mathrm{opt}}. \tag{52}$$

Finally, we reconstruct $\mathbf{c}$ from $\tilde{\mathbf{c}}_{\mathrm{opt}}$.

Similarly to the previous case of the hypercardioid, if no additional constraints except (36) are imposed, (52) reduces to the solution of the symmetric unconstrained supercardioid in [6].

In Section VI-B, two design examples of a third-order asymmetric supercardioid are presented and compared to the symmetric design.

The theoretical framework of the asymmetric CDMAs which has been developed in this section, may provide much more flexible design of broadband beamformers based on CDMAs with improved performance level. In the next section, we present a general framework for a practical implementation of Nth-order asymmetric CDMAs, whose inputs are the analytical optimal asymmetric beampatterns derived in this section.

V. Practical Design for Asymmetric CDMAs

In this section, we present a general framework for a practical implementation of asymmetric CDMAs. One way to implement CDMAs is by the conventional time-domain approach [6]. This approach is limited by some aspects like the flexibility to forming different patterns and the ability to handle white noise amplification. Instead, we may employ here a more general approach in the frequency domain as described in details in [14], [33]. The major advantages of the frequency-domain design with respect to the traditional time-domain design are the following. 1) It is easier to design different patterns by using only the null and attenuation information. 2) The high-pass response of the time-domain implementation is inherently compensated by the design in the frequency domain. 3) It enables to apply a minimum-norm approach that can maximize the WNG with a given number of sensors, i.e., the frequency-domain framework is suitable for any number of sensors, while the traditional approach is suitable only for the case of $M = N + 1$. 4) It is well-known that frequency-domain processing of broadband signals has several advantages with respect to time-domain broadband processing by means of lower computational complexity and high convergence rate [38], and in some applications, beamforming will serve as a pre-processing stage followed by a second adaptive processing stage implemented more efficiently in the frequency-domain (e.g., de-reverberation, speech enhancement). Due to all these reasons, we propose to implement asymmetric CDMAs by the following approach.

The solutions for the optimal asymmetric hypercardioid and supercardioid, derived in the previous section, yield the vector $\mathbf{c}$ which is used to build the corresponding theoretical beampattern (28), which is a trigonometric polynomial with $2N$ zeros. Recall that during the design of the asymmetric hypercardioid and the asymmetric supercardioid we impose in (38) up to $L \leq 2N$ directional attenuation constraints denoted by $\{\theta_l\}_{l=1}^{L}$. We use these L directions to the following processing, and calculate $2N - L$ additional null directions of the beampattern, by numerical standard methods of finding roots. At the end of this process we have the column vector:

$$\boldsymbol{\theta} = [\theta_1, \ldots, \theta_{2N}]^T \tag{53}$$

of length $2N$, where these directions are with respect to a steering angle of $\theta_{\mathrm{s}} = 0^{\circ}$. The next step is to implement the beamformer with the attenuation directions specified by the vector $\boldsymbol{\theta}$. Note that the rotation to any different steering angle is straightforward.

The following design generalizes the derivation of CDMAs proposed in [33]. The main contribution of [33] is a symmetric design of CDMAs for the angle $\theta = 0^{\circ}$ which can be steered directly to each of the other sensor angles, ψ_m, $m = 2, \ldots, M$, without any change in the properties of the beamformer. Herein, we present a general asymmetric design which enables to steer to all azimuthal directions without any change in the beampattern, WNG, DF, or FBR. This solution coincides with the solution in [33] for the case of symmetric design and steering to one of the sensors directions, ψ_m, $m = 1, 2, \ldots, M$, therefore the solution proposed in [33] is considered as a particular case.

Nth-order asymmetric CDMAs can be designed with at least $2N + 1$ microphones for the general case where the steering angle can be each of the azimuthal directions [33]. This is because in the general Nth-order design we enforce $2N$ attenuation constraints and one distortionless constraint. For the case of symmetric design with steering to ψ_m, $m = 1, 2, \ldots, M$, only $2N$ microphones are sufficient because the symmetry constraint enables to reduce the total number of the attenuation constraints.

In order to design the asymmetric CDMAs, we have to apply the distortionless constraint in the desired signal direction, θ_{s}, i.e.,

$$\mathbf{d}^H(\omega, \theta_{\mathrm{s}})\, \mathbf{h}(\omega) = 1, \tag{54}$$

where

$$\mathbf{h}(\omega) = [H_1(\omega)\ H_2(\omega)\ \cdots\ H_M(\omega)]^T \tag{55}$$

is a vector containing the complex weights of the beamformer, and $\mathbf{d}(\omega, \theta)$ is the steering vector (6). Then, we have $2N$ additional directional constraints of the form

$$\mathbf{d}^H(\omega, \theta_{\mathrm{s}} + \theta_i)\, \mathbf{h}(\omega) = \nu_i, \quad i = 1, \ldots, 2N, \tag{56}$$

where ν_i, $i = 1, 2, \ldots, 2N$, are the attenuation parameters, with $0 \leq \nu_i \leq 1$, and $\theta_i \in \boldsymbol{\theta}$, $i = 1, 2, \ldots, 2N$, with $\theta_1 \neq \theta_2 \neq \cdots \neq \theta_{2N}$, are the corresponding directions where the attenuations are desired ($\nu_l = g_l, \forall l = 1, \ldots, L$, and $\nu_l = 0, \forall l = L + 1, \ldots, 2N$). Combining these $2N + 1$ constraints together, we get the following linear system to solve

$$\mathbf{D}_{N,M}(\omega, \theta_{\mathrm{s}}, \boldsymbol{\theta})\mathbf{h}(\omega) = \boldsymbol{\nu}, \tag{57}$$

where

$$\mathbf{D}_{N,M}(\omega, \theta_{\mathrm{s}}, \boldsymbol{\theta}) = \begin{bmatrix} \mathbf{d}^H(\omega, \theta_{\mathrm{s}}) \\ \mathbf{d}^H(\omega, \theta_{\mathrm{s}} + \theta_1) \\ \vdots \\ \mathbf{d}^H(\omega, \theta_{\mathrm{s}} + \theta_{2N}) \end{bmatrix} \tag{58}$$

is a $(2N + 1) \times M$ matrix and the vector $\boldsymbol{\nu}$ is

$$\boldsymbol{\nu} = \begin{bmatrix} 1 & \nu_1 & \nu_2 & \cdots & \nu_{2N} \end{bmatrix}^T. \tag{59}$$

Practically, it is desired to add a constraint on the squared norm of the solution vector $\mathbf{h}(\omega)$, which is inversely proportional to the WNG and minimizes the objective function

$$J(\mathbf{h}(\omega)) = \|\boldsymbol{\nu} - \mathbf{D}_{N,M}(\omega, \theta_{\mathrm{s}}, \boldsymbol{\theta})\mathbf{h}(\omega)\|_2^2 + \eta \|\mathbf{h}(\omega)\|_2^2, \tag{60}$$

where $\|\cdot\|_2$ is ℓ_2-norm. The small positive parameter η is usually set according to the desired WNG, where the WNG is given by [33]

$$\mathcal{W}[\mathbf{h}(\omega)] = \frac{\left|\mathbf{h}^H(\omega)\, \mathbf{d}(\omega, \theta_{\mathrm{s}})\right|^2}{\mathbf{h}^H(\omega)\, \mathbf{h}(\omega)}, \tag{61}$$

which is a measure indicating the array gain in the presence of uncorrelated white noise. It also indicates the sensitivity of the array to model mismatch errors [35].

Assuming $M \geq 2N + 1$, and using the method of Lagrange multipliers we can obtain the regularized pseudo-inverse

solution:

$$\mathbf{h}(\omega) = \mathbf{P}^{\dagger}_{\mathbf{D}_{N,M}}(\omega, \theta_{\mathrm{s}}, \boldsymbol{\theta})\boldsymbol{\nu}, \tag{62}$$

where

$$\mathbf{P}^{\dagger}_{\mathbf{X}} = \left[\mathbf{X}^H\mathbf{X} + \eta\mathbf{I}\right]^{-1}\mathbf{X}^H \tag{63}$$

is the pseudo-inverse of a matrix $\mathbf{X}$, and $\mathbf{I}$ is the identity matrix with the same dimensions as the matrix $\mathbf{X}^H\mathbf{X}$.

Although (62) depends on frequency and its structure is different from the traditional time-domain DMAs [6], it indeed leads to an equivalent implementation of differential beamforming with frequency-invariant beampatterns as presented in [14] for the linear symmetric case, and in [33] for the circular case. Specifically, the authors of [14] show analytically that for each ω satisfying the DMAs model assumption (7), the beampattern obtained by the frequency-domain design is very similar to the theoretical one obtained by the time-domain design. Moreover, the simulations presented in the next section support this claim. Therefore, as both the frequency- and time- domain designs are equivalent, the proposed frequency-domain design yields a frequency-invariant differential beamformer.

Notice that for a design of beampatterns with multiple nulls in the same directions like dipole and cardioid, $\mathbf{D}_{N,M}(\omega, \theta_{\mathrm{s}}, \boldsymbol{\theta})$ becomes singular. In order to overcome this singularity, we can add constraints on the derivatives of the steering vector in directions of the multiple nulls. Derivative constraints are known in the literature and have recently also been applied to DMAs [39].

VI. Simulations

In this section, we demonstrate some of the benefits of the asymmetric design with respect to the traditional symmetric one. We start with two examples demonstrating how to design optimal second-order asymmetric hypercardioid according to Section IV-B, and optimal third-order asymmetric supercardioid according to Section IV-C. Then, we proceed to present two more examples of a practical design of CDMAs according to Section V. The first practical design example is for the simple case of a first-order asymmetric design, and the second example is for higher order.

A. An Optimal Second-Order Asymmetric Hypercardioid

Fig. 2 shows beampatterns of two design examples for the second-order asymmetric hypercardioid, obtained by the calculation of (41). In the first example (a), we choose two null directions at $\theta_1 = 60^\circ$ and $\theta_2 = 110^\circ$. Three beampatterns are compared. The first is the asymmetric beampattern (blue solid line), the second is the corresponding symmetric version beampattern (black dashed line), i.e., the beampattern obtained by enforcing the above two null directions plus the symmetry constraint. The third beampattern is the second-order unconstrained symmetric hypercardioid (red circles line) which is obtained by maximization of the DF without any constraints on the null directions [6]. The symmetric design achieves slightly narrower mainbeam but much higher sidelobes with respect to the asymmetric design and the unconstrained symmetric design. In the second example (b), we choose two null directions at $\theta_1 = 120^\circ$, and $\theta_2 = 295^\circ$. Table I shows the DF (31) obtained by each of the designs for both examples. One can see that while in the asymmetric design, the DF approaches the optimal value, the symmetric design achieves much lower DF with respect to the theoretical upper bound associated with the unconstrained symmetric design. In both examples we choose $\theta_{\mathrm{s}} = 0^\circ$, yet, the modification to any direction is straightforward.

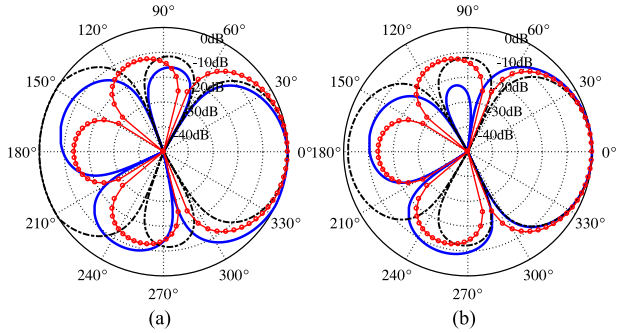

Fig. 2. Beampatterns for the second-order asymmetric hypercardioid CDMAs (blue solid line) and its symmetric version (black dashed line). The red circles line is the second-order unconstrained symmetric hypercardioid [6]. (a) $\theta_1 = 60^\circ, \theta_2 = 110^\circ$. (b) $\theta_1 = 120^\circ, \theta_2 = 295^\circ$.

TABLE I
Directivity Factor Achieved by Each of the Designs of a Second-Order Hypercardioid

$\mathcal{D}$[dB]	(a)	(b)
Asymmetric	6.22	6.70
Symmetric	2.63	5.50
Unconstrained symmetric	6.98	6.98

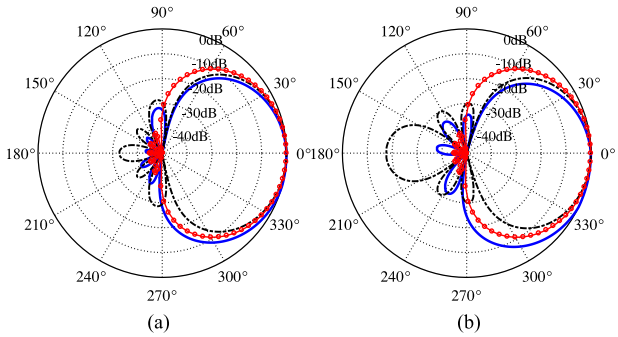

Fig. 3. Beampatterns for the third-order asymmetric supercardioid CDMAs (blue solid line) and its symmetric version (black dashed line). The red circles line is the third-order unconstrained symmetric supercardioid [6]. (a) $\theta_1 = 80^\circ$, $\theta_2 = 120^\circ, \theta_3 = 155^\circ$. (b) $\theta_1 = 75^\circ, \theta_2 = 105^\circ, \theta_3 = 220^\circ$.

B. An Optimal Third-Order Asymmetric Supercardioid

Fig. 3 shows beampatterns of two design examples for the third-order asymmetric supercardioid, obtained by the calculation of (52). In the first example (a), we choose three null directions at $\theta_1 = 80^\circ$, $\theta_2 = 120^\circ$, and $\theta_3 = 155^\circ$. Three beampatterns are compared. The first is the asymmetric beampattern (blue solid line), the second is the corresponding symmetric

TABLE II
FRONT-TO-BACK-RATIO ACHIEVED BY EACH OF THE DESIGNS OF A THIRD-ORDER SUPERCARDIOID

$\mathcal{F}$[dB]	(a)	(b)
Asymmetric	35.0	33.8
Symmetric	29.7	19.8
Unconstrained symmetric	40.6	40.6

version beampattern (black dashed line), i.e., the beampattern obtained by enforcing the above three null directions plus the symmetry constraint. The third beampattern is the third-order unconstrained symmetric supercardioid (red circles line) which is obtained by maximization of the FBR without any constraints on the null directions [6]. The symmetric design achieves slightly narrower mainbeam but much higher sidelobes with respect to the asymmetric design and the unconstrained symmetric design. In the second example (b), we choose three null directions at $\theta_1 = 75^\circ, \theta_2 = 105^\circ$, and $\theta_3 = 240^\circ$. Table II shows the FBR (42) obtained by each of the designs in each example. One can see that while in the asymmetric design, the FBR approaches the optimal value, the symmetric design achieves much lower FBR with respect to the unconstrained symmetric design. These examples show that the proposed asymmetric design achieves superior results with respect to the symmetric design, as more flexibility is allowed in the null directions. We now demonstrate two examples of a practical design of asymmetric CDMAs, based on what we have presented in Section V.

C. Asymmetric Implementation of First-Order CDMAs

Herein, we present a design example of a first-order asymmetric hypercardioid and compare it to the symmetric design. We choose the radius of the array to be $r = 0.75$ cm and $M = 3$ which leads to a sensor spacing of $\delta \approx 1.3$ cm. For this choice of parameters, we get a small value of $\varpi \approx 0.15 \ll M$ justifying the approximation on (13). Let us assume that the steering angle is $\theta_s = 0^\circ$ and we would like to null signals arriving from $\theta_1 = 95^\circ$. Substituting these constraints into (39), and solving (41), we get the optimal coefficients vector, $\mathbf{c}$ (33), used to calculate the analytical first-order asymmetric beampattern (28):

$$\mathcal{B}_1(\theta) = 0.261 + 0.738\cos\theta - 0.1977\sin\theta, \tag{64}$$

which is a first-order trigonometric polynomial with two roots. The second root is $\theta_2 = 235^\circ$. Fig. 4 shows the analytical beampattern of the first-order asymmetric design (blue solid line), the symmetric version (black dashed line), i.e., the beampattern for the case that $\theta_1 = 95^\circ$ and $\theta_2 = 265^\circ$, and also the first-order unconstrained symmetric hypercardioid (red circles line), which was obtained in [6] for a null at $\theta_1 = 120^\circ$. The asymmetric design leads to the desired beampattern which is similar to the unconstrained hypercardioid but with a slight bias in the azimuth in order to satisfy both the distortionless and the null constraints. In contrast to the asymmetric design, the symmetric design achieves a beampattern with a much wider and higher sidelobe.

The null directions calculated from (28) are then used to design the first-order asymmetric CDMA filter vector $\mathbf{h}(\omega)$

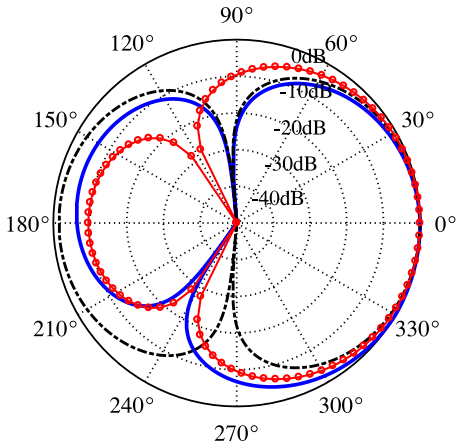

Fig. 4. A first-order asymmetric hypercardioid beampattern (blue solid line) obtained by (28) and a symmetric beampattern (black dashed line) obtained by imposing symmetry, for the case of $M = 3$ sensors, and desired null at $\theta_1 = 95^\circ$. The red circles line is the first-order unconstrained hypercardioid [6].

according to (62), where we used the regularization parameter $\eta = 10^{-8}$. We calculate the designed beampattern defined as

$$\begin{aligned}\mathcal{B}[\mathbf{h}(\omega), \theta] &= \mathbf{h}^H(\omega)\mathbf{d}(\omega, \theta) \\ &= \sum_{m=1}^{M} H_m^*(\omega) e^{j\varpi\cos(\theta - \psi_m)},\end{aligned} \tag{65}$$

where $\mathbf{d}(\omega, \theta)$ is the steering vector (6). While (65) is the designed beampattern, (28) is the theoretical asymmetric beampattern.

Fig. 5 shows $\mathcal{B}[\mathbf{h}(\omega), \theta]$ for the first-order asymmetric hypercardioid (a)–(b), the symmetric hypercardioid (c)–(d), and the first-order unconstrained hypercardioid (e)–(f), for different frequencies and steering angles. The black dashed line is the designed beampattern (65), while the blue circles line is the analytical beampattern (28). One can see that the beampatterns in both cases are frequency-invariant and also rotation-invariant in the azimuthal axis. These properties make the circular geometry very suitable to processing broadband signals which can come from any azimuthal direction.

Note that when the steering angle coincides with one of the other sensors' directions (i.e., ψ_2, ψ_3), the filter coefficients vector, $\mathbf{h}(\omega)$ (62) is a permutation of the vector designed for the case of $\theta_s = \psi_1 = 0^\circ$. This observation implies that the proposed solution is general, which includes also the previous solution [33] as a particular case, as this property is satisfied also by the solution derived in [33].

Fig. 6 shows the WNG and DF as a function of frequency for the practical design of a first-order asymmetric hypercardioid (blue solid line), the symmetric hypercardioid (black dashed line), and the first-order unconstrained symmetric hypercardioid (red circles line). The DF for the case of a cylindrically diffuse noise is calculated similarly to (31) as

$$\mathcal{D}[\mathbf{h}(\omega)] = \frac{2\pi}{\int_0^{2\pi} |\mathcal{B}[\mathbf{h}(\omega), \theta]|^2 d\theta}. \tag{66}$$

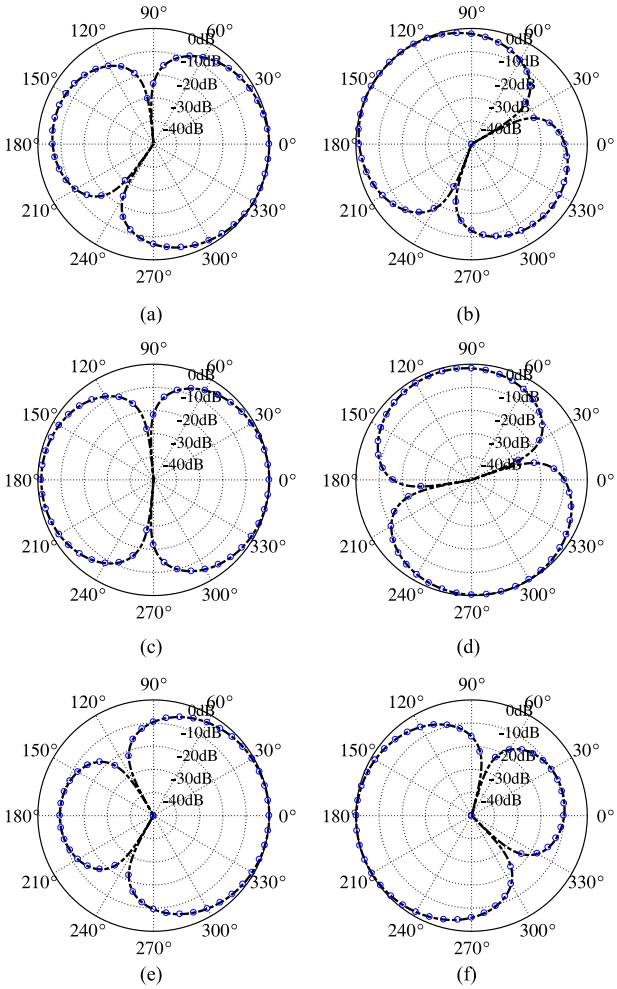

Fig. 5. Beampatterns of the first-order asymmetric hypercardioid using CDMAs with $M = 3$ sensors for different steering angles and frequencies. (a) $\theta_s = 0°$, $f = 600$ Hz. (b) $\theta_s = 155°$, $f = 2400$ Hz. Beampatterns of the corresponding first-order symmetric design. (c) $\theta_s = 0°$, $f = 1000$ Hz. (d) $\theta_s = 285°$, $f = 3200$ Hz . Beampatterns of the first-order unconstrained symmetric hypercardioid. (e) $\theta_s = 0°$, $f = 900$ Hz, (f) $\theta_s = 195°$, $f = 2100$ Hz . The black dashed line is the designed beampattern (65), while the blue circles line is the analytical beampattern (28).

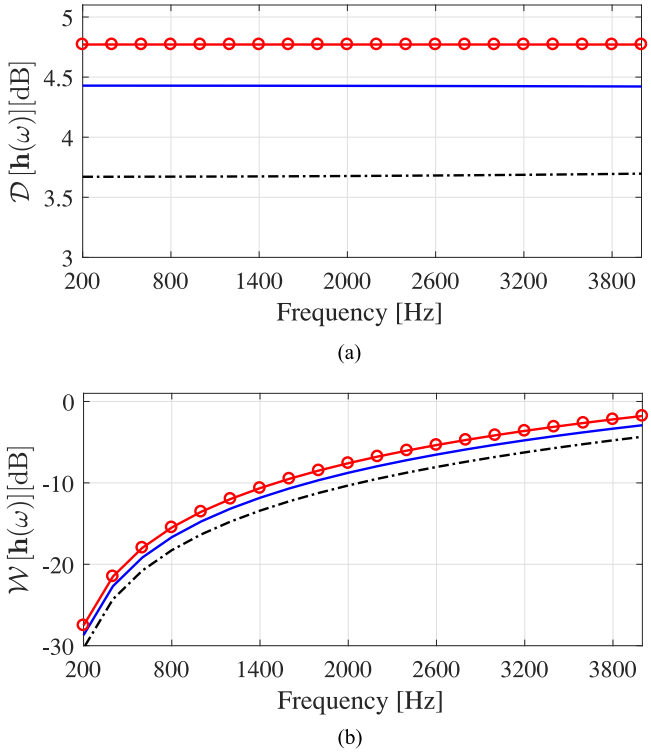

Fig. 6. DF (a) and WNG (b) vs. frequency for the first-order asymmetric hypercardioid (blue solid line), the optimal unconstrained symmetric hypercardioid (red circles line), and the symmetric design (black dashed line) with $M = 3$ sensors.

The performance of the asymmetric design is very close to that of the unconstrained symmetric hypercardioid, while the non-optimal symmetric design achieves lower DF. The WNG of all three considered methods has similar behavior and is quite poor in low frequencies which is a drawback of DMAs. In the next subsection, we show how a higher-order asymmetric design can be exploited to achieve better WNG, and discuss about other ways to improve it even further.

The results presented in this section demonstrate the benefit of the asymmetric design, which can be exploited for the circular geometry. For this simple first-order example, it is obvious that higher DF can be obtained with respect to the standard symmetric design for a given required null direction.

D. Second-Order CDMAs With More Than Two Imposed Nulls

In this section, we present a design example for the second-order hypercardioid and exemplify another advantage of the asymmetric framework. Traditionally, in the Nth-order DMAs symmetric design up to N distinct nulls could be imposed. Herein, we show that the proposed asymmetric design may enable more than N imposed nulls for order N. This is an important property of the asymmetric design as it enables to design reduced-order CDMAs for a given number of nulls and achieve a much larger WNG with respect to the symmetric design. Note that one of the effective ways to improve the WNG is by increasing the number of microphones [15], which is limited in some practical applications. Therefore, the following example is of a great relevance for real-world applications.

Let us assume that we are limited only to $M = 5$ microphones and we are interested to impose three nulls at $\theta_1 = 60°$, $\theta_2 = 190°$, and $\theta_3 = 275°$. We choose the radius of the array to be $r = 0.75$ cm which leads to a sensor spacing of $\delta \approx 0.88$ cm. While for the asymmetric design, five microphones are sufficient, for the traditional symmetric design, we need at least third-order CDMA and seven microphones, therefore, for the symmetric design, we use $M = 7$ sensors and keep the value of $r = 0.75$ cm which leads to $\delta \approx 0.65$ cm. We compare between the second-order asymmetric design and the third-order symmetric design.

First, we need to find an expression for the analytical beampattern for asymmetric hypercardioid with the above directions by using (41). From (41), we get the optimal coefficients vector, $\mathbf{c}$ (33), and substitute it into the analytical asymmetric beampattern (28). We get the following second-order asymmetric

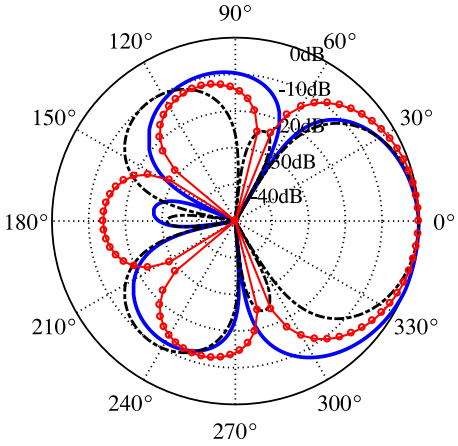

Fig. 7. An asymmetric second-order hypercardioid beampattern (blue solid line) obtained by (28) for the case of three imposed nulls and $M = 5$ microphones. Also presented the corresponding third-order symmetric beampattern (black dashed line) for the case of $M = 7$ sensors, and desired nulls at $\theta_1 = 60°$, $\theta_2 = 190°$, and $\theta_3 = 275°$. The red circles line is the second-order unconstrained hypercardioid [6].

beampattern:

$$\mathcal{B}_2(\theta) = 0.16 + 0.482\cos\theta + 0.358\cos(2\theta) - 0.13\sin\theta - 0.126\sin(2\theta), \tag{67}$$

which is a second-order trigonometric polynomial with four roots. The fourth root is $\theta_2 = 156°$. Fig. 7 shows the analytical beampattern of the second-order asymmetric design (blue solid line), the corresponding third-order symmetric design (black dashed line) which enforces nulls in the above directions, and the second-order unconstrained symmetric hypercardioid (red circles line), which was obtained for nulls at $\theta_1 = 72°$, and $\theta_2 = 144°$, and their corresponding symmetric directions. The symmetric design has narrower mainbeam as it is a third-order design while the asymmetric design is a second-order design.

We can now use these outputs in order to design the practical second-order asymmetric CDMA using (62), with the same regularization parameter $\eta = 10^{-8}$. Fig. 8 shows the beampattern of the second-order asymmetric hypercardioid (a)–(b), the third-order symmetric hypercardioid (c)–(d), and the second-order unconstrained symmetric hypercardioid, for different frequencies and steering angles. The black dashed line is the designed beampattern (65), while the blue circles line is the analytical beampattern (28).

Fig. 9 shows the WNG and the DF as a function of frequency for the second-order asymmetric hypercardioid (blue solid line), the third-order symmetric design (black dashed line), and the second-order unconstrained symmetric hypercardioid (red circles line). Two more designs are presented for comparison. The first is the third-order symmetric design for the case of $M = 15$ and $\delta = 0.65$ cm, leading to $r = 1.57$ cm (magenta diamonds line), and a larger array. The second (green triangles line) is for the case of $M = 20$ microphones and the radius is $r = 0.75$ cm, meaning that the array is more dense but of the same size like the original one. As expected, while

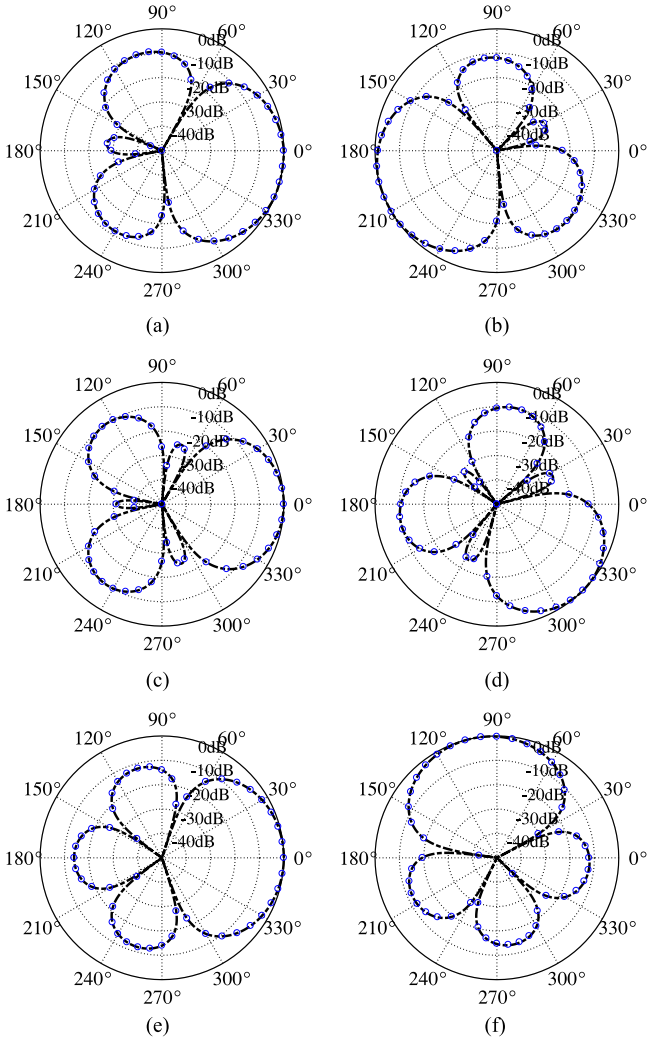

Fig. 8. Beampatterns of the second-order asymmetric hypercardioid CDMAs with $M = 5$ sensors and three imposed nulls for different steering angles and frequencies. (a) $\theta_s = 0°$, $f = 800$ Hz. (b) $\theta_s = 215°$, $f = 1800$ Hz. Beampatterns of the corresponding third-order symmetric design with $M = 7$ sensors. (c) $\theta_s = 0°$, $f = 200$ Hz. (d) $\theta_s = 315°$, $f = 1900$ Hz. Beampatterns of the second-order unconstrained symmetric hypercardioid. (e) $\theta_s = 0°$, $f = 1300$ Hz. (f) $\theta_s = 100°$, $f = 3500$ Hz. The black dashed line is the designed beampattern (65), while the blue circles line is the analytical beampattern (28).

the third-order symmetric design achieves higher directivity by less than 1 dB with respect to the other second-order designs, the second-order design achieves superior WNG of up to 15 dB with respect to the third-order design. Moreover, comparing the performances of the asymmetric design and the second-order unconstrained design, the loss in performance is negligible even though three nulls were imposed instead of two. Regarding the third-order symmetric design with larger M, we can see that increasing only the number of sensors (green triangles line) provides a small improvement, but still far from the performance of the second-order designs. The other case of a larger array (magenta diamonds line), yields better performance, but at the price of a larger physical array which can be problematic in some scenarios where strong limitations on the available space exist. Therefore, we conclude that the proposed asymmetric design can be used to resolve the trade-off

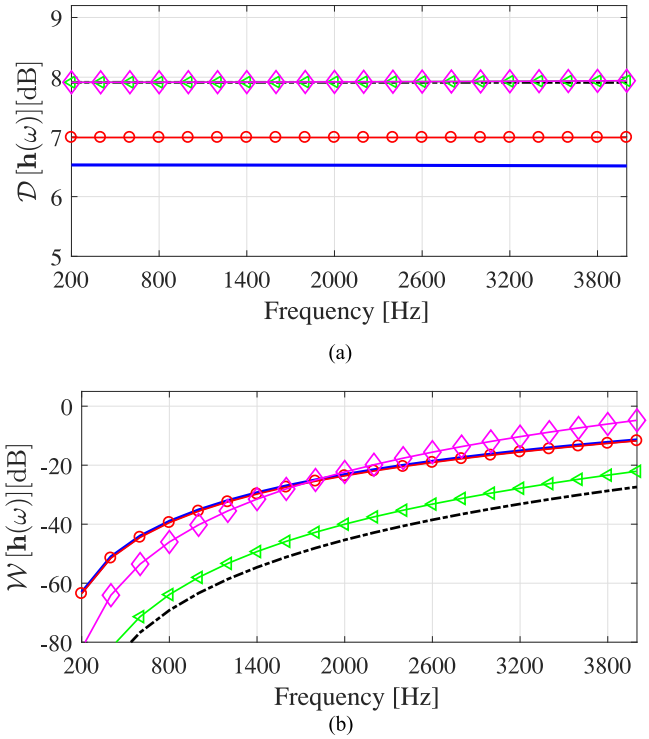

Fig. 9. DF (a) and WNG (b) vs. frequency for the second-order asymmetric hypercardioid (blue solid line), the second-order unconstrained symmetric hypercardioid (red circles line) with $M = 5$ sensors, and the third-order symmetric design (black dashed line) with $M = 7$ sensors. Also presented the third-order symmetric design (magenta diamonds line) with $M = 15$ sensors and larger array (element spacing, $\delta = 0.65$ cm), and the third-order symmetric design (green triangles line) with $M = 20$ sensors and the same size of original array ($r = 0.75$ cm).

between high directivity and robustness associated with the design of CDMAs.

Note that even the improved results of the asymmetric design presented in Fig. 9 are inadequate for real scenarios, as the WNG at low frequencies is much lower. Further improvement of the WNG involves methods which are based either on increasing the number of sensors [14] or more advanced regularization methods [35], [40], where the regularization parameter depends on frequency. We did not include such improvements, which can be applied either for the asymmetric design or the traditional symmetric one, in the scope of this paper since we have concentrated on the improvement obtained by the utilization of the asymmetric model rather than the symmetric one.

Finally, Fig. 10 shows from a top view the beampattern versus frequency and θ for the asymmetric second-order hypercardioid CDMA designed in this subsection. As expected, the frequency-invariance property can be clearly seen. One can identify the main lobe and the two dominant sidelobes in accordance with Fig. 8(a) and (b), which presents up to azimuthal rotation, two slices of Fig. 10 corresponding to frequencies $f_1 = 800$ Hz and $f_2 = 1800$ Hz.

The examples presented in this section illustrate the benefits of the proposed asymmetric model to achieve better performance and control of the null directions during the design process of CDMAs.

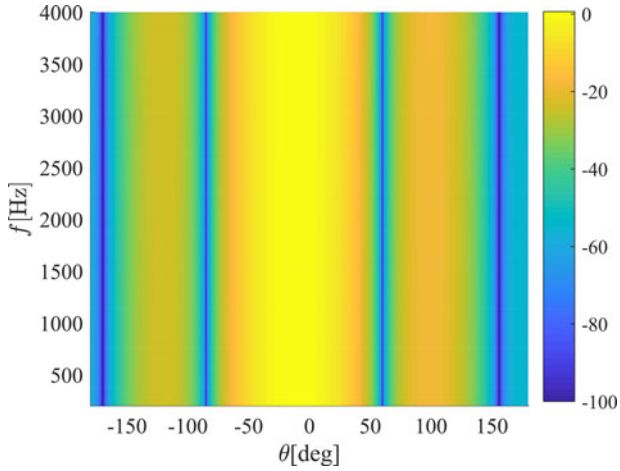

Fig. 10. A top view of the beampattern versus frequency and θ for the asymmetric second-order hypercardioid CDMA implemented in Section VI-D.

VII. Conclusions

We have presented an analytical model for asymmetric CDMAs, which includes the traditional symmetric model as a particular case. This model includes the derivation of the analytical Nth-order asymmetric beampattern, and asymmetric versions of two commonly-used optimal beampatterns, namely the hypercardioid and the supercardioid. A simple general Nth-order asymmetric practical design in the frequency-domain for any number of microphones is also presented. Simulation results demonstrate some of the benefits achieved by the asymmetric model with respect to the traditional symmetric model for DMAs. Specifically, the asymmetric model allows more degrees of freedom which can be exploited to achieve better performance in terms of WNG, DF, and FBR. Moreover, for a given number of desired null directions, the asymmetric model may allow reduced order of CDMAs with respect to the symmetric model leading to an improved robustness to array imperfections. Therefore, this concept is of a great importance for some real-world CDMAs based beamforming applications since it allows smaller and more robust designs with respect to the regular symmetric design.

Appendix
Proof of the Equivalence Between (23) and (28)

In order to prove the equivalence, we may use the formula:

$$\sin(N\theta) = \sum_{k=0}^{N} \binom{N}{k} \cos^k\theta \sin^{N-k}\theta \sin\left[\frac{(N-k)\pi}{2}\right], \tag{68}$$

which can be obtained from Euler Formula and the Binomial theorem. We consider the following four cases.

Case 1: N and k are both even. Thus, $N - k = 2l$ is also even and l is an integer number. In that case, the coefficient of each term in (68) is

$$\sin\left[\frac{(N-k)\pi}{2}\right] = \sin\left[\frac{(2l)\pi}{2}\right] \equiv 0. \tag{69}$$

Case 2: N and k are both odd. Thus, $N-k=2l$ is even. In that case we also get that each term in (68) is equal to zero.

Case 3: N is even and k is odd. Thus, $N-k$ is also odd. In that case:

$$\begin{aligned}\cos^k\theta\sin^{N-k}\theta &= \cos\theta\cos^{k-1}\theta\sin^{N-k}\theta\\ &= \cos\theta\left(\cos^2\theta\right)^{\frac{k-1}{2}}\sin\theta\left(\sin^2\theta\right)^{\frac{N-k-1}{2}}\\ &= \cos\theta\left(1-\sin^2\theta\right)^{\frac{k-1}{2}}\sin\theta\left(\sin^2\theta\right)^{\frac{N-k-1}{2}}\\ &= \cos\theta\sin\theta\mathcal{P}_{\frac{N-2}{2}}\left(\sin^2\theta\right)\\ &= \cos\theta\sin\theta\left(p_0+p_1\sin^2\theta\right.\\ &\quad\left.+\ p_2\sin^4\theta+\cdots+p_{\frac{N-2}{2}}\sin^{N-2}\right)\\ &= \cos\theta\left(p_0\sin\theta+p_1\sin^3\theta\right.\\ &\quad\left.+\ p_2\sin^5\theta+\cdots+p_{\frac{N-2}{2}}\sin^{N-1}\theta\right),\end{aligned}\tag{70}$$

where $\mathcal{P}_\alpha(x)$ is a polynomial in x of degree α.

Case 4: N is odd and k is even. Thus, $N-k$ is also odd. In that case:

$$\begin{aligned}\cos^k\theta\sin^{N-k}\theta &= \left(1-\sin^2\theta\right)^{\frac{k}{2}}\sin^{N-k}\theta\\ &= \mathcal{P}_{\frac{k}{2}}\left(\sin^2\theta\right)\sin\theta\mathcal{P}_{\frac{N-k-1}{2}}\left(\sin^2\theta\right)\\ &= \sin\theta\mathcal{P}_{\frac{N-1}{2}}\left(\sin^2\theta\right)\\ &= p_0\sin\theta+p_1\sin^3\theta\\ &\quad+p_2\sin^5\theta+\cdots+p_{\frac{N-2}{2}}\sin^N\theta.\end{aligned}\tag{71}$$

From (70) and (71), one can see that all the terms required to express $\sin(N\theta)$ are exactly the terms at the second and third summations of (23).

Regarding the terms $\cos(N\theta)$. It is well known that

$$\cos(N\theta)=T_N(\cos\theta),\tag{72}$$

where $T_N(\cdot)$ is the Nth Chebyshev polynomial of the first kind [41], which has the recurrence relation:

$$T_{N+1}(\cos\theta)=2\cos\theta\times T_N(\cos\theta)-T_{N-1}(\cos\theta),\tag{73}$$

with

$$T_0(\cos\theta)=1,\ T_1(\cos\theta)=\cos\theta.\tag{74}$$

Thus, $\cos(N\theta)$ can be expressed as a sum of powers of $\cos\theta$, which is exactly the terms at the first summation of (23). Therefore, we can conclude that (23) and (28) are both equivalent for all N.

REFERENCES

[1] H. Cox, R. M. Zeskind, and T. Kooij, "Practical supergain," *IEEE Trans. Acoust., Speech, Signal Process.*, vol. ASSP-34, no. 3, pp. 393–398, Jun. 1986.

[2] M. Crocco and A. Trucco, "Design of robust superdirective arrays with a tunable tradeoff between directivity and frequency-invariance," *IEEE Trans. Signal Process.*, vol. 59, no. 5, pp. 2169–2181, May 2011.

[3] H. H. Olson, "Gradient microphones," *J. Acoust. Soc. Amer.*, vol. 17, pp. 192–198, Jan. 1946.

[4] G. M. Sessler and J. E. West, "Directional transducers," *IEEE Trans. Audio Electroacoust.*, vol. 19, no. 1, pp. 19–23, Mar. 1971.

[5] G. W. Elko and A. T. N. Pong, "A simple adaptive first-order differential microphone," in *Proc. IEEE Workshop Appl. Signal Process. Audio Acoust.*, 1995, pp. 169–172.

[6] G. W. Elko, "Superdirectional microphone arrays," in *Acoustic Signal Processing for Telecommunication*, S. L. Gay and J. Benesty, Eds. Boston, MA USA: Kluwer, 2000, ch. 10, pp. 181–237.

[7] G. W. Elko, "Differential microphone arrays," in *Proc. in Audio Signal Process. Next-Gener. Multimedia Commun. Syst.*, Y. Huang and J. Benesty, Eds. Norwell, MA, USA: Kluwer, 2004, ch. 2, pp. 11–65.

[8] T. D. Abhayapala and A. Gupta, "Higher order differential-integral microphone arrays," *J. Acoust. Soc. Amer.*, vol. 127, pp. 227–233, May 2010.

[9] M. Kolundžija, C. Faller, and M. Vetterli, "Spatiotemporal gradient analysis of differential microphone arrays," *J. Audio Eng. Soc.*, vol. 59, pp. 20–28, Feb. 2011.

[10] M. Buck, "Aspects of first-order differential microphone arrays in the presence of sensor imperfections," *Eur. Trans. Telecommun.*, vol. 13, pp. 115–122, Mar. 2002.

[11] R. M. M. Derkx and K. Janse, "Theoretical analysis of a first-order azimuth-steerable superdirective microphone array," *IEEE Trans. Audio, Speech, Lang. Process.*, vol. 17, pp. 150–162, Jan. 2009.

[12] H. Teutsch and G. W. Elko, "First- and second-order adaptive differential microphone arrays," in *Proc. 7th Int. Workshop Acoust. Echo Noise Control*, 2001, pp. 57–60.

[13] E. De Sena, H. Hacihabiboğlu, and Z. Cavetković, "On the design and implementation of higher order differential microphones," *IEEE Trans. Audio, Speech, Lang. Process.*, vol. 20, no. 1, pp. 162–174, Jan. 2012.

[14] J. Benesty and J. Chen, *Study and Design of Differential Microphone Arrays*. Berlin, Germany: Springer, 2012.

[15] L. Zhao, J. Benesty, and J. Chen, "Design of robust differential microphone arrays," *IEEE Trans. Audio, Speech, Lang. Process.*, vol. 22, no. 10, pp. 1455–1464, Oct. 2014.

[16] C. Pan, J. Benesty, and J. Chen, "Design of robust differential microphone arrays with orthogonal polynomials," *J. Acoust. Soc. Amer.*, vol. 138, no. 2, pp. 1079–1089, Aug. 2015.

[17] H. Zhang, J. Chen, and J. Benesty, "Study of nonuniform linear differential microphone arrays with the minimum-norm filter," *Appl. Acoust.*, vol. 98, pp. 62–69, May 2015.

[18] C. Pan, J. Chen, and J. Benesty, "Theoretical analysis of differential microphone array beamforming and an improved solution," *IEEE Trans. Audio, Speech, Lang. Process.*, vol. 23, no. 11, pp. 2093–2105, Nov. 2015.

[19] Y. Buchris, I. Cohen, and J. Benesty, "First-order differential microphone arrays from a time-domain broadband perspective," in *Proc. Int. Workshop Acoust. Signal. Enhanc. (IWAENC)*, 2016, pp. 1–5

[20] G. Huang, J. Benesty, and J. Chen, "Design of robust concentric circular differential microphone arrays," *J. Acoust. Soc. Amer.*, vol. 141, no. 5, pp. 3236–3249, 2017.

[21] C. Pan, J. Chen, and J. Benesty, "Performance study of the MVDR beamformer as a function of the source incident angle," *IEEE/ACM Trans. Audio, Speech, Lang. Process.*, vol. 22, no. 1, pp. 67–79, Jan. 2014.

[22] H. Teutsch and W. Kellerman, "Acoustic source detection and localization based on wavefield decomposition using circular microphone arrays," *J. Acoust. Soc. Amer.*, vol. 120, no. 5, pp. 2724–2736, Nov. 2006.

[23] M. Wax and J. Sheinvald, "Direction finding of coherent signals via spatial smoothing for uniform circular arrays," *IEEE Trans. Antennas. Propag.*, vol. 42, no. 5, pp. 613–620, May 1994.

[24] C. P. Mathews and M. D. Zoltowski, "Eigenstructure techniques for 2-D angle estimation with uniform circular arrays," *IEEE Trans. Signal Process.*, vol. 42, no. 9, pp. 2395–2407, Sep. 1994.

[25] E. Tiana-Roig, F. Jacobsen, and E. F. Grande, "Beamforming with a circular microphone array for localization of environmental noise sources," *J. Acoust. Soc. Amer.*, vol. 128, pp. 3535–3542, 2010.

[26] B. Friedlander, "The MVDR beamformer for circular arrays," in *Proc. 34th Asilomar Conf. Signals, Syst., Comput.*, vol. 1, Nov. 2000, pp. 25–29.

[27] P. Ioannides and C. A. Balanis, "Uniform circular and rectangular arrays for adaptive beamforming applications," *IEEE Antennas Wireless Propagat. Lett.*, vol. 4, pp. 351–354, 2005.

[28] Y. L. Ma, Y. Yang, Z. He, K. Yang, C. Sun, and Y. Wang, "Theoretical and practical solutions for high-order superdirectivity of circular sensor arrays," *IEEE Trans. Ind. Electron.*, vol. 60, no. 1, pp. 203–209, Jan. 2013.

[29] S. C. Chan and K. S. Pun, "On the design of digital broadband beamformer for uniform circular array with frequency invariant characteristics," in *Proc. IEEE Int. Symp. Circuits Syst.,* Phoenix, AZ, USA May 2002, vol 1, pp. 693–696.

[30] H. H. Chen, S. C. Chan, and K. L. Ho, "Adaptive beamforming using frequency invariant uniform concentric circular arrays," *IEEE Trans. Circuits Syst. I, Reg. Papers*, vol. 54, no. 9, pp. 1938–1949, Sep. 2007.
[31] S. C. Chan and H. H. Chen, "Uniform concentric circular arrays with frequency-invariant characteristics - theory, design, adaptive beamforming and DOA estimation," *IEEE Trans. Signal Process.*, vol. 55, no. 1, pp. 165–177, Jan. 2007.
[32] X. Zhang, W. Ser, Z. Zhang, and A. K. Krishna, "Selective frequency invariant uniform circular broadband beamformer," *EURASIP J. Adv. Signal Process.*, pp. 1–11, 2010.
[33] J. Benesty, J. Chen, and I. Cohen, *Design of Circular Differential Microphone Arrays*. Berlin, Germany: Springer, 2015.
[34] Y. Buchris, I. Cohen, and J. Benesty, "Analysis and design of time-domain first-order circular differential microphone arrays," in *Proc. 22nd Int. Congr. Acoust.*, 2016, pp. 1–5.
[35] H. L. Van-trees, *Detection, Estimation and Modulation Theory, Part IV—Optimum Array Processing*. New York, NY, USA: Wiley, 2002.
[36] S. Doclo and M. Moonen, "Design of far-field and near-field broadband beamformers using eigenfilters," *Signal Process.*, vol. 83, pp. 2641–2673, Dec. 2003.
[37] S. C. Pei and C. C. Tseng, "A new eigenfilter based on total least squares error criterion," *IEEE Trans. Circuits Syst. I*, vol. 48, pp. 699–709, Jun. 2001.
[38] Y. Avargel and I. Cohen, "System identification in the short-time Fourier transform domain with crossband filtering," *IEEE Trans. Audio, Speech, Lang. Process.*, vol. 15, no. 4, pp. 1305–1319, May 2007.
[39] C. Pan, J. Benesty, and J. Chen, "Design of directivity patterns with a unique null of maximum multiplicity," *IEEE/ACM Trans.Audio, Speech, Lang. Process.*, vol. 24, no. 2, pp. 226–235, Feb. 2016.
[40] R. Berkun, I. Cohen, and J. Benesty, "Combined beamformers for robust broadband regularized superdirective beamforming," *IEEE/ACM Trans. Audio, Speech, Lang. Process.*, vol. 23, no. 5, pp. 877–886, May 2015.
[41] M. Abramowitz and I. A. Stegun, *Handbook of Mathematical Functions With Formulas, Graphs, and Mathematical Tables*. New York, NY, USA: Dover, 1970.

Yaakov Buchris (M'10) received the B.Sc. and M.Sc. degrees in electrical engineering in 2005 and 2011, respectively, from the Technion—Israel Institute of Technology, Haifa, Israel, where he is currently working toward the Ph.D. degree in electrical engineering.

Since 2002, he has been with RAFAEL, Advanced Defense Systems Ltd, Haifa, Israel, as a Research Engineer in the underwater acoustic communication group. Since 2005, he has also been a Teaching Assistant and a Project Supervisor with the Communications Lab and the Signal and Image Processing Lab, Department of Electrical Engineering, Technion—Israel Institute of Technology. His research interests include statistical signal processing, adaptive filtering, digital communications, and array processing.

Israel Cohen (M'01–SM'03–F'15) received the B.Sc. (Summa Cum Laude), M.Sc., and Ph.D. degrees in electrical engineering from the Technion—Israel Institute of Technology, Haifa, Israel, in 1990, 1993 and 1998, respectively.

He is currently a Professor of electrical engineering with the Technion—Israel Institute of Technology, Haifa, Israel.

From 1990 to 1998, he was a Research Scientist with RAFAEL Research Laboratories, Haifa, Israel, Ministry of Defense. From 1998 to 2001, he was a Postdoctoral Research Associate with the Computer Science Department, Yale University, New Haven, CT, USA. In 2001, he joined the Electrical Engineering Department of the Technion. He is a coeditor of the Multichannel Speech Processing Section of the *Springer Handbook of Speech Processing* (Springer, 2008), a coauthor of *Noise Reduction in Speech Processing* (Springer, 2009), a Coeditor of *Speech Processing in Modern Communication: Challenges and Perspectives* (Springer, 2010), and a General Cochair of the 2010 International Workshop on Acoustic Echo and Noise Control. He was a Guest Editor of the *European Association for Signal Processing Journal on Advances in Signal Processing* Special Issue on Advances in Multimicrophone Speech Processing and the *Elsevier Speech Communication Journal* a Special Issue on Speech Enhancement. His research interests include statistical signal processing, analysis and modeling of acoustic signals, speech enhancement, noise estimation, microphone arrays, source localization, blind source separation, system identification, and adaptive filtering.

Dr. Cohen was a recipient of the Alexander Goldberg Prize for Excellence in Research, and the Muriel and David Jacknow Award for Excellence in Teaching. He was a Member of the IEEE Audio and Acoustic Signal Processing Technical Committee. He was an Associate Editor of the IEEE TRANSACTIONS ON AUDIO, SPEECH, AND LANGUAGE PROCESSING and IEEE SIGNAL PROCESSING LETTERS, and as a Member of the IEEE Speech and Language Processing Technical Committee.

Jacob Benesty received the Master's degree in microwaves from Pierre & Marie Curie University, Paris, France, in 1987, and the Ph.D. degree in control and signal processing from Orsay University, Orsay, France, in April 1991. During the Ph.D. degree (from November 1989 to April 1991), he worked on adaptive filters and fast algorithms with the Centre National d'Etudes des Telecommunications, Paris, France. From January 1994 to July 1995, he worked with Telecom Paris University on multichannel adaptive filters and acoustic echo cancellation. From October 1995 to May 2003, he was first a Consultant and then a Member of the Technical Staff at Bell Laboratories, Murray Hill, NJ, USA. In May 2003, he joined the University of Quebec, INRS-EMT, Montreal, QC, Canada, as a Professor. He is also a Visiting Professor with the Technion—Israel Institute of Technology, Haifa, Israel, and an Adjunct Professor with Aalborg University, Aalborg, Denmark. In particular, he was the Lead Researcher with Bell Labs who conceived and designed the world-first real-time hands-free full-duplex stereophonic teleconferencing system. Also, he conceived and designed the world-first PC-based multi-party hands-free full-duplex stereo conferencing system over IP networks. He is the inventor of many important technologies. His research interests include in signal processing, acoustic signal processing, and multimedia communications.

Dr. Benesty is the Editor of the book series Springer Topics in Signal Processing. He has co-authored and co-edited/co-authored numerous books in the area of acoustic signal processing. He was the General Chair and Technical Chair of many international conferences. He was a member of several IEEE technical committees. Four of his journal papers were awarded by the IEEE Signal processing Society. In 2010, he received the Gheorghe Cartianu Award from the Romanian Academy.